Available online at www.sciencedirect.com
ScienceDirect
Journal of Power Sources 162 (2006) 294–301
JOURNAL OF POWER SOURCES
www.elsevier.com/locate/jpowsour

Corrosion behavior of 316L stainless steel and $Zr_{75}Ti_{25}$ bulk amorphous alloy in simulated PEMFC anode environment in a solution containing 12.5 ppm H_2SO_4 + 1.8 ppm HF at 25 and 80 °C

Shize Jin [a,*], Edward Ghali [a], Arianna T. Morales [b]

[a] *Department of Mining, Metallurgical and Materials Engineering, Laval University, Quebec, Que. G1K7P4, Canada*
[b] *General Motors R&D Center, Materials & Processes Laboratory, 30500 Mound Road, Warren, MI 48090-9055, USA*

Received 24 March 2006; received in revised form 22 June 2006; accepted 23 June 2006
Available online 9 August 2006

Abstract

Metallic alloys have been considered for the fabrication of bipolar plates for polymer electrolyte membrane fuel cells (PEMFC). The corrosion behavior of 316L stainless steel (316L) and $Zr_{75}Ti_{25}$ bulk amorphous alloy (AB) in PEMFC environments was studied using polarization resistance and electrochemical impedance spectroscopy (EIS) methods. The results showed that under natural corrosion conditions, the amorphous bulk alloy had a corrosion resistance close to that of 316L stainless steel. In all other fuel cell environments studied, the corrosion rate of AB was lower than that of 316L.

Keywords: Stainless steel; Amorphous alloy; Corrosion; Electrochemical impedance

1. Introduction

The most widely used material for polymer electrolyte membrane fuel cells (PEMFC) bipolar plates is graphite. The cells volumetric size and the power/volume ratio could be significantly improved by using bipolar plates made of metal alloys. Metallic bipolar plates could provide additional advantages such as cheaper material cost, good electrical and thermal conductivity, and a variety of manufacturing processes.

Several authors [1–13] have investigated the possibility of using stainless steel for the fabrication of bipolar plates due to its excellent corrosion resistance in some environments. All these results indicate that the stainless steel corrosion resistance should be increased to make possible its use as plate material in PEMFC. The corrosion of the alloys in their current state would lead to loss of electrons and metallic ions to the electrolyte and to the poisoning of the polymer membrane [14].

The general objective of the work was to evaluate the corrosion of 316L stainless steel and compare it with that of a $Zr_{75}Ti_{25}$ bulk amorphous alloy (AB). AB was selected for its lack of grain boundaries and thus, improved resistance to grain boundary corrosion. The 316L steel properties are the baseline requirements for metallic bipolar plates in fuel cell environments.

2. Experiment

The corrosion behavior of the alloys in anodic conditions was determined by potentiostatic polarization followed by measurements of the corrosion current and rate using polarization resistance methods. The free corrosion behavior of 316L and AB alloy was examined since the plates remain in contact with the electrolyte during cell shut down. Their corrosion potential (E_{corr}), corrosion current (i_{corr}) and corrosion rate ($Rate_{corr}$) in the acid solution were recorded using potentiodynamic methods.

2.1. Materials and specimens preparation

The corrosion behavior of small specimens of 316L and $Zr_{75}Ti_{25}$ bulk amorphous alloy plate was tested. Samples were embedded in acrylic resin leaving an exposed area of about 1.5 cm^2 for electrochemical measurements. The specimens were polished with 600 grit SiC abrasive paper, washed with de-ionized water and dried before electrochemical evaluation.

* Corresponding author. Tel.: +1 418 656 2131x4838; fax: +1 418 656 5343.
E-mail address: shize.jin@gmn.ulaval.ca (S. Jin).

0378-7753/$ – see front matter © 2006 Elsevier B.V. All rights reserved.
doi:10.1016/j.jpowsour.2006.06.060

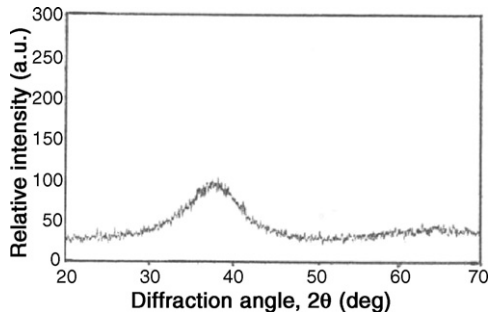

Fig. 1. X-ray diffraction pattern showing the amorphous nature of $Zr_{75}Ti_{25}$ alloy plate.

2.2. Experimental conditions

A 1-l double-walled cell containing 800 ml of the acid solution (pH 3.2) was used as electrochemical test cell. The solution contained 12.5 ppm of H_2SO_4 and 1.8 ppm of HF in reactive grade water (18 MΩ) and its temperature (25 ± 0.2 or 80 ± 0.5 °C) was controlled by a flow of water at constant temperature within the double wall. Humidified H_2 was bubbled and the solution was stirred magnetically during the experiments. The counter electrode (CE) was made of platinum foil and a saturated calomel electrode acted as the reference electrode (RE). A saturated KCl salt bridge was used to maintain a constant distance of ~4 mm between the reference and the working electrode (WE). The three electrodes were mounted in a Teflon holder and the distance between WE and CE was fixed at 20 mm.

Polarization curves were taken using an EG&G Princeton Applied Research 273 potentiostat/galvanostat using a sweep rate of 0.2 mV s^{-1} and controlled by an IBM computer. 352 SoftCorr III™ was used for polarization data acquisition and processing. Electrochemical impedance was measured using a Solartron 1255 HF frequency response analyzer and a Solartron 1286 electrochemical interface in the frequency range from 10 kHz to 0.1 Hz. The amplitude of the sinusoidal signals was 30 mV (rms) for polarization, and 50 mV (rms) for free corrosion at open circuit potential measurements. Zplot™ was used for acquisition of the impedance data. The Nyquist plots of the impedance data were analyzed using Zview™ to calculate charge-transfer resistance and double layer capacity during the corrosion process.

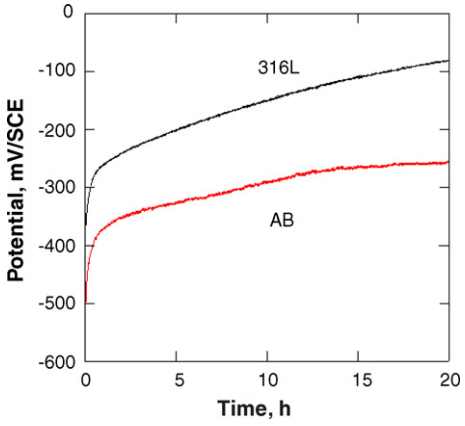

Fig. 2. Evolution of the corrosion potential of 316L and AB alloy in the acid solution bubbled with H_2 at 25 °C.

3. Results and discussion

3.1. Microstructure characterization

The X-ray diffraction pattern of the $Zr_{75}Ti_{25}$ alloy plate presents a broad band in the diffraction angle range 2θ between 35° and 45° (Fig. 1). The characteristic peaks corresponding to the crystalline phases of Zr and Ti are absent and this confirms that the $Zr_{75}Ti_{25}$ alloy has an amorphous nature.

3.2. Corrosion behavior in the acid solution bubbled with H_2 at 25 °C

3.2.1. At open circuit potential

3.2.1.1. Polarization results. Fig. 2 shows the evolution of E_{corr} with time at open circuit potential for 316L and AB. The corrosion potential of 316L was always more positive than that

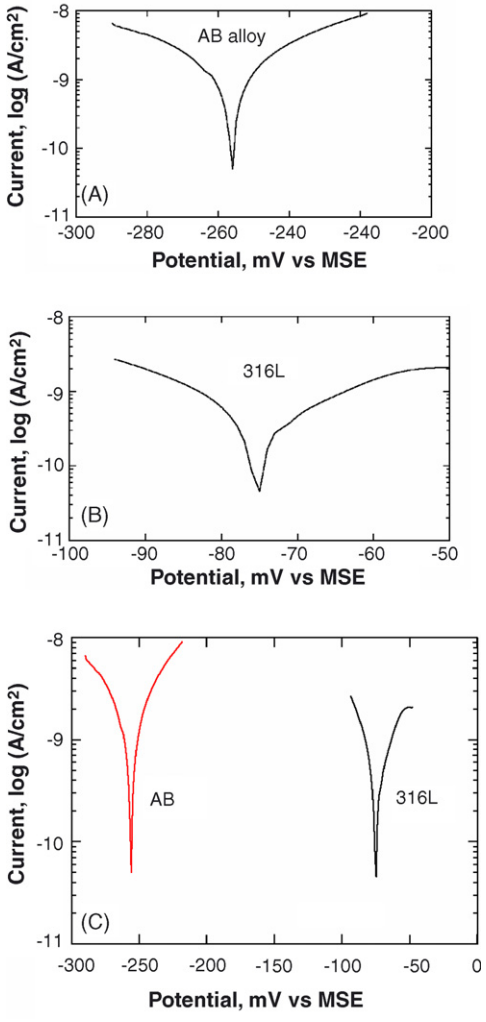

Fig. 3. Linear polarization curves of AB alloy (A) and 316L (B) after 20 h of immersion in the acid solution bubbled with H_2 at 25 °C. (C) A comparison of the two curves.

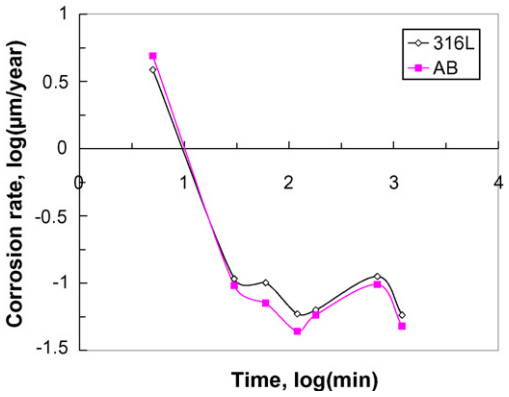

Fig. 4. Twenty hours evolution of the corrosion rate of 316L stainless steel and AB alloy in the acid solution bubbled with H_2 at 25 °C.

of AB alloy. After 20 h of immersion, a potential sweep was performed in a potential range of $E_{corr} \pm 25$ mV at a scan rate of 0.2 mV s^{-1}. Typical linear polarization curves of AB alloy and 316L are shown in Fig. 3. E_{corr}, i_{corr} and corrosion rates in micrometer per year were calculated based on these curves using linear polarization resistance method. The results showed that the corrosion rates of the two alloys were almost the same as seen in Fig. 4, which shows the corrosion rates of the two alloys as a function of time during 20 h immersion. Table 1 shows the corrosion rate after 3 and 20 h immersions.

3.2.1.2. Electrochemical impedance spectroscopy (EIS) results. A typical Nyquist plot [15] taken on an AB specimen after 4 h immersion is shown in Fig. 5. The open circles represent experimental data. The solid line is a simulation curve obtained using the fitting parameters from the equivalent circuit (insert drawing in Fig. 5) that describes the corrosion process of the AB alloy in the acid solution. In the equivalent circuit, R_s is solution resistance between the reference electrode capillary and the working

Table 1
Corrosion rate of 316L stainless steel and AB alloy in the acid solution bubbled with H_2 at 25 °C

Sample	Corrosion rate (μm $year^{-1}$)	
	3 h	20 h
316L	0.063	0.058
AB	0.058	0.048

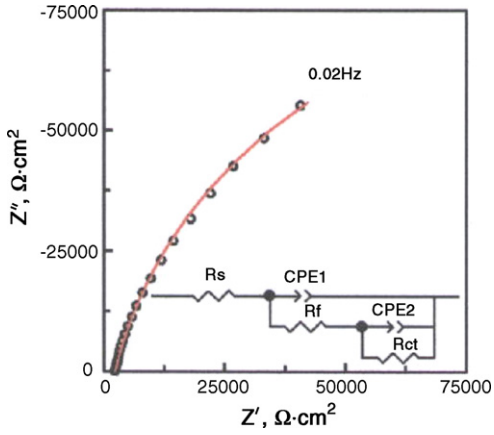

Fig. 5. Nyquist plot of the AB alloy immersed in the acid solution bubbled with H_2 at 25 °C for 4 h.

electrode surface; R_{ct} is the charge-transfer resistance and CPE is a constant related to the double layer capacity (C_{dl}) or to the oxide film capacity (C_f) on the working electrode surface.

Fig. 6 shows Bode plots [16] of the impedance diagram of 316L and AB after 24 h immersion in the acid solution bubbled with H_2 at 25 °C. The Z value of AB was higher than that of 316L, especially in the low frequency range. This implies that

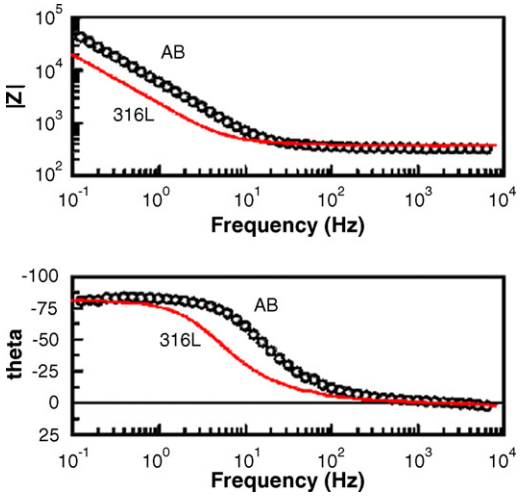

Fig. 6. Bode plots of the ac impedance diagram of 316L and AB alloy after 24 h of immersion in the acid solution bubbled with H_2 at 25 °C.

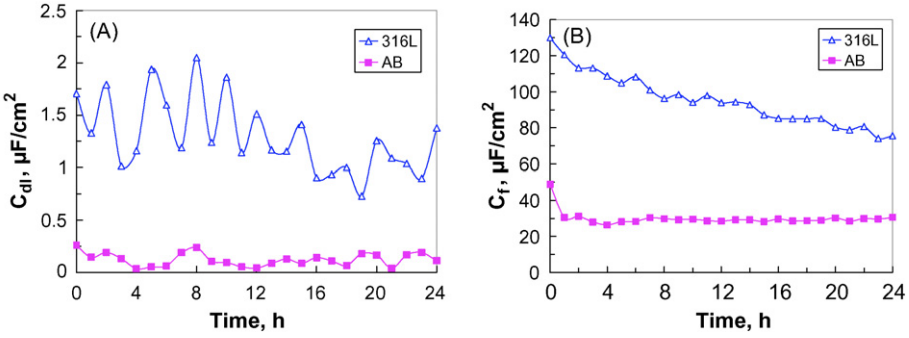

Fig. 7. Time dependence of C_{dl} (A) and C_f (B) of 316L and AB alloy in the acid solution bubbled with H_2 at 25 °C.

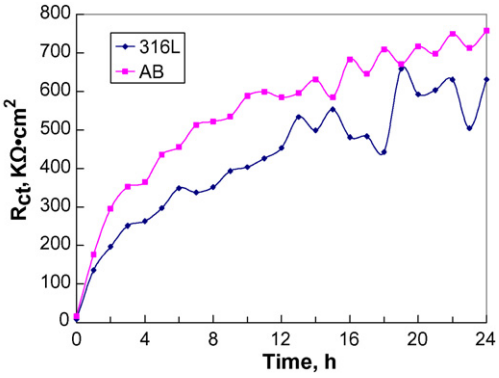

Fig. 8. Time dependence of the charge-transfer resistance of the corrosion process of 316L and AB alloy in the acid solution bubbled with H_2 at 25 °C.

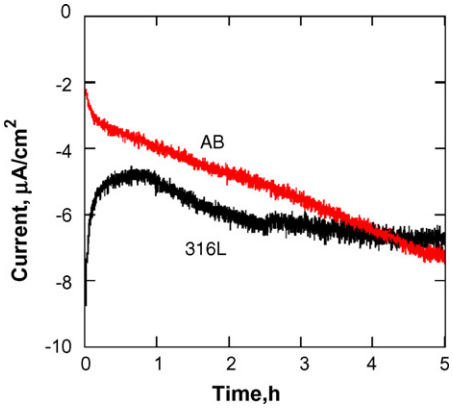

Fig. 9. Time polarization curves of 316L and AB alloy at a constant potential of −444 mV versus SCE (−400 mV vs. Ag/AgCl) in the acid solution bubbled with H_2 at 25 °C.

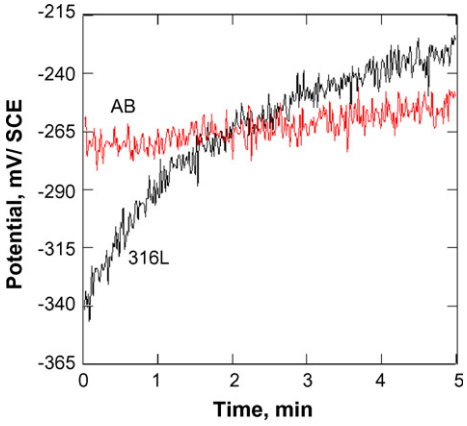

Fig. 10. Potential decay of 316L and AB alloy during the first 5 min after potentiostatic polarization at −444 mV versus SCE (−400 mV vs. Ag/AgCl) in the acid solution bubbled with H_2 at 25 °C.

the corrosion impedance of AB was higher than that of 316L. The phase angle theta (θ) for AB was slightly bigger than that of 316L, especially in the medium frequency range. This indicated that the C_{dl} of 316L was bigger than that of AB alloy, because θ is inversely proportional to capacity. Calculations of the C_{dl} values from the Nyquist plots confirmed this statement as showed in Fig. 7. The C_{dl} difference between 316L and AB ally was probably due to surface differences between the two alloys. A higher C_{dl} implies a higher surface roughness or porosity. In general, stainless steel has small C_{dl} when its oxide film is continuous, nonporous, insoluble and self-healing. In this case, the lack of oxygen in the solution and the presence of hydrofluoric acid prevented stabilization of the oxide film which in turn accounted for the higher C_{dl}. In the case of AB alloy, the amorphous structure increased the resistance to the HF attack and thus, led to the lower C_{dl} value. This suggestion is supported also by the calculation of the oxide film capacity (C_f) shown in Fig. 7B which reveals that the C_f of 316L decreased with immersion time, while that of AB alloy remained rather stable. The fact that the C_f value of 316L was always bigger than that of AB alloy resulted probably from the difference of the dielectric constants and the thicknesses of the oxide films of the two alloys [15].

Fig. 8 compares the charge-transfer resistance as a function of time for 316L and AB at open circuit potential. At the beginning, the two alloys showed similar R_{ct} values; but later the AB alloy exhibited higher R_{ct} than 316L. At the end of 24 h immersion, the charge-transfer resistance of AB was 757 kΩ cm^2, while that of 316L was 631 kΩ cm^2. These results indicated that the metallic atoms in the AB alloy had more difficulty to loose electrons than those in 316L. Thus, AB exhibited a higher corrosion resistance than 316L.

3.2.2. *Electrochemical behavior of 316L and AB alloy in simulated PEMFC anode environment at 25 °C*

3.2.2.1. Polarization results. Fig. 9 displays the potentiostatic curves of 316L and AB alloy polarized at a potential of −444 mV versus SCE in the acid solution bubbled with H_2. The 316L stainless steel showed higher polarization current density during the first 4 h immersion. However, the polarization current of AB increased more quickly with time than that of 316L. The current difference between the two materials became negligible after 4 h of polarization.

The potential decay was recorded immediately at the end of the potentiostatic polarization, as shown in Fig. 10. The free corrosion potential of 316L was lower than that of AB during the first 2 min. This can be explained by the quantity of the adsorbed hydrogen formed during the cathodic polarization. Since stainless steel contains iron and nickel and the formation of their hydrides is thermodynamically favored, a part of the hydrogen stayed on the metal in the form of hydride or adsorbed hydrogen (H_{ads}), phenomenon that has been previously reported by many researchers [7,14,17,18]. Instead, in AB which mainly contained Zr and Ti, it was the molecular hydrogen that formed

Table 2
Corrosion potential and current, polarization resistance and corrosion rate after 5 h of potentiostatic polarization followed by 5 min potential decay in the same conditions

Sample	E_{corr} (mV versus SCE)	i_{corr} (μA cm^{-2})	R_p (kΩ cm^2)	Rate$_{corr}$ (μm year^{-1})
316L	−226	0.158	137	1.98
AB	−250	0.092	236	1.34

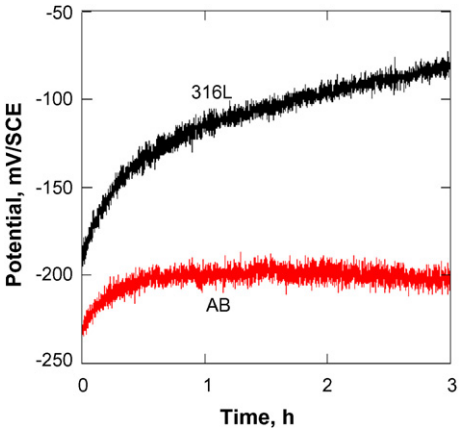

Fig. 11. Three hours potential decay of 316L and AB alloy after 5 h potentiostatic polarization at −444 mV versus SCE (−400 mV vs. Ag/AgCl) followed by 5 min E decay in the acid solution bubbled with H_2 at 25 °C under fuel cell conditions at 25 °C.

and released from the metal during polarization. The quantity of the adsorbed hydrogen formed during the AB cathodic polarization was lower than in the case of 316L. When the cathodic potential was removed, the hydride and/or H_{ads} on 316L began to oxidize at lower corrosion potential and higher corrosion current than those of the AB alloy, as shown in Table 2 and Fig. 10.

After 2.5 min of potential decay, the corrosion potential of 316L overstepped that of the AB alloy and after that the difference in potential between the two alloys became more and more important with time. After 3 h, the E_{corr} of 316L was about 120 mV more positive than that of AB alloy (Fig. 11); and the corrosion rate of the former was a little higher than that of the latter as seen Table 3. However, for both alloys the corrosion current dropped more than 21 times after 3 h of potential decay as seen in Tables 2 and 3. Thus, in the short term of potential decay after the cathodic polarization, the corrosion current measured was related to the oxidation current of the adsorbed hydrogen formed during the polarization on the stainless steel surface. When the adsorbed hydrogen was exhausted, the measured corrosion current was actually the real corrosion current of the metal.

3.2.2.2. EIS results. Fig. 12 shows the Nyquist plots of electrochemical impedance of the two alloys polarized at −444 mV versus SCE. The 316L impedance plot is composed of two semi-circles while that of the AB alloy contains only one semi-circle, which indicates that the corrosion mechanisms of the two alloys were different. Calculation of the equivalent circuit parameters showed that in 316L the resistance of the first step

Table 3
Corrosion potential and current, polarization resistance and corrosion rate after 5 h of potentiostatic polarization followed by 3 h of potential decay in the acid solution at 25 °C

Sample	E_{corr} (mV versus SCE)	i_{corr} (μA cm^{-2})	R_p (kΩ cm^2)	Rate$_{corr}$ (μm year^{-1})
316L	−80	0.008	2731	0.09
AB	−202	0.0055	3982	0.06

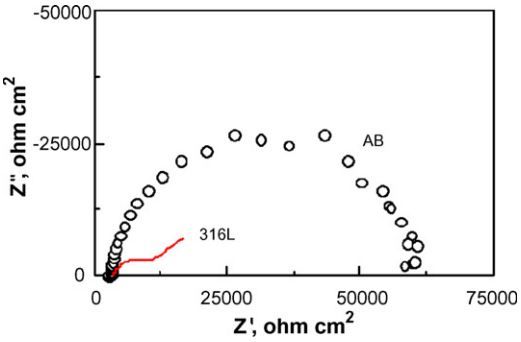

Fig. 12. Nyquist plots of the electrochemical impedance of 316L (continuous line) and AB alloy (open circles) polarized at a constant potential of −444 mV versus SCE (−400 mV vs. Ag/AgCl) for 3 h in the acid solution bubbled with H_2 at 25 °C under fuel cell conditions at 25 °C.

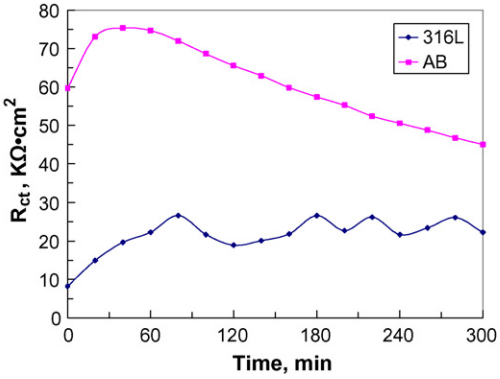

Fig. 13. Time dependence of the charge-transfer resistances of the electrode reaction on 316L and AB alloy polarized at constant potential of −444 mV versus SCE (−400 mV vs. Ag/AgCl) in acid solution bubbled with H_2 at 25 °C.

(3.4 kΩ cm^2) of the hydrogen reduction reaction was smaller than that of the second step (25.4 kΩ cm^2). In the case of AB, the first step (57.1 kΩ cm^2) was much more difficult than the second (0.5 kΩ cm^2), and the two semi-circles could not be distinguished. Thus, the rate of hydrogen reduction reaction on the $Zr_{75}Ti_{25}$ bulk amorphous alloy was controlled by the first step of the cathodic reaction.

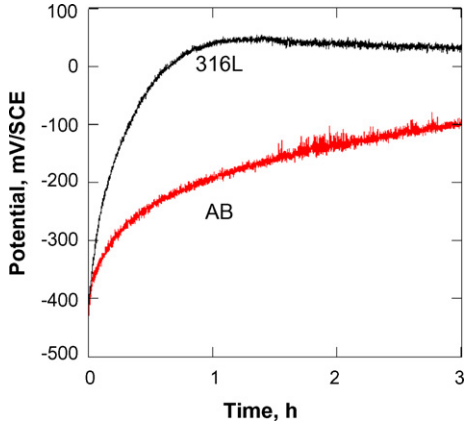

Fig. 14. Three hours evolution of corrosion potential of 316L and AB alloy at open circuit potential in the acid solution bubbled with H_2 at 80 °C.

Table 4
Corrosion potential and current, polarization resistance and corrosion rate of 316L and AB alloy after 3 h of immersion in the acid solution bubbled with H_2 at 80 °C

Sample	E_{corr} (mV versus SCE)	i_{corr} ($\mu A\,cm^{-2}$)	R_p ($k\Omega\,cm^2$)	$Rate_{corr}$ ($\mu m\,year^{-1}$)
316L	35	0.038	573	0.35
AB	−100	0.017	1274	0.2

The charge-transfer resistance of 316L was lower than that of AB alloy, as shown in Fig. 13. As the R_{ct} is inversely proportional to the current, it is clear that the polarization current of 316L was higher than that of AB. These results are in accordance with the potentiostatic polarization studies. The two curves in Fig. 13 got closer to each other with time showing the same tendency as in Fig. 9. The $Zr_{75}Ti_{25}$ bulk amorphous alloy became more active for the cathode reaction and finally reached a similar current level than 316L. The slight increase of the current on AB was due to the activation of the surface that could include reduction of the passive oxide layer. In the 316L surface instead, the current stayed stable mainly due to the reduction of hydrogen ions.

3.3. Corrosion behavior in the acid solution bubbled with H_2 at 80 °C

3.3.1. At open circuit potential

3.3.1.1. Polarization results. The corrosion potential of 316L was always more positive than that of AB. After 3 h of immersion, the corrosion potential of 316L reached a stable value while that of AB was still increasing, as seen in Fig. 14. The corrosion potentials and currents, polarization resistances and corrosion rates of 316L and AB alloy after 3 h of immersion in the acid solution are given in Table 4. At this temperature, 316L had a corrosion rate of 0.35 $\mu m\,year^{-1}$, while that of AB alloy was only 0.2 $\mu m\,year^{-1}$. Compared to the corrosion rates of 316L and AB alloy at 25 °C which were 0.063 and 0.058 $\mu m\,year^{-1}$, respectively, it can be concluded that rising temperature resulted in increase of corrosion rates of both 316L and AB, and that AB alloy had lower corrosion rate than 316L at the two temperatures.

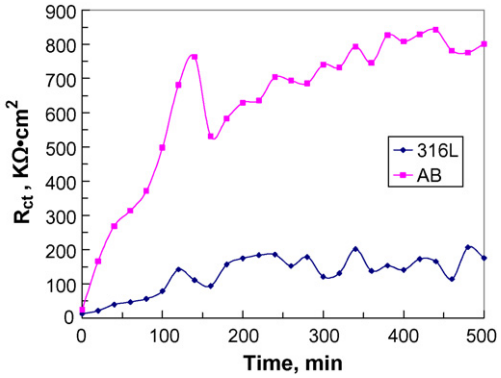

Fig. 15. Time dependence of charge-transfer resistance of the corrosion process of 316L and AB alloy at open circuit potential in the acid solution bubbled with H_2 at 80 °C.

3.3.1.2. EIS results. The charge-transfer resistances of both 316L and AB alloy increased with time and the R_{ct} value of AB was always higher than that of 316L, as shown in Fig. 15. The C_{dl} and C_f values of 316L were bigger than those of AB (Fig. 16). It is admitted that high double layer capacity in certain conditions signifies higher roughness of surface or/and higher porosity or/and higher geometric area [19,20]. So, the higher double layer capacity of 316L than that of AB alloy means that the surface of 316L stainless steel was more porous or/and rougher than that of AB alloy. The oxide film capacity of 316L was always much bigger than that of AB alloy; the former decreased with time while the latter value was rather stable as shown in Fig. 16B. This means that the passive film of AB alloy was more stable in these conditions.

3.3.2. Electrochemical behavior of 316L and AB alloy in simulated PEMFC anode environment at 80 °C

3.3.2.1. Polarization results. Potentiostatic polarization at −444 mV versus SCE followed by measurements of E_{corr} and i_{corr} was carried out to evaluate the corrosion behavior of the two materials in a simulated anode environment at 80 °C. Results of 5 h potentiostatic polarizations are shown in Fig. 17. 316L showed higher current densities than AB during polarization. The polarization current of AB decreased slowly from 3.8 to 3.2 $\mu A\,cm^{-2}$ during the experiments. Instead, the initial 316L

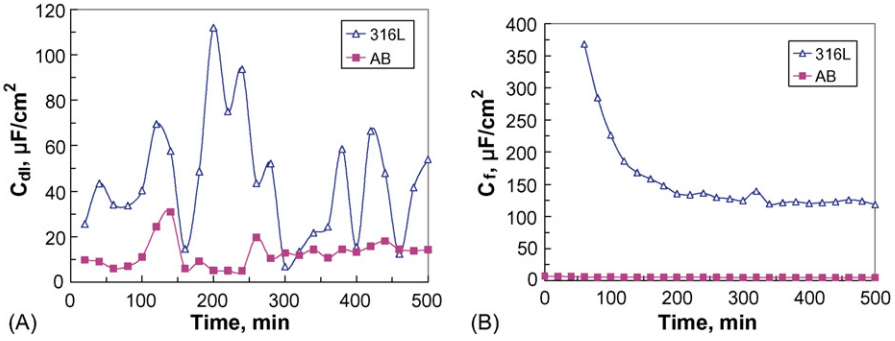

Fig. 16. Time dependence of double layer capacity C_{dl} (A) and oxide film capacity C_f (B) of the corrosion process of 316L and AB alloy at open circuit potential in the acid solution bubbled with H_2 at 80 °C.

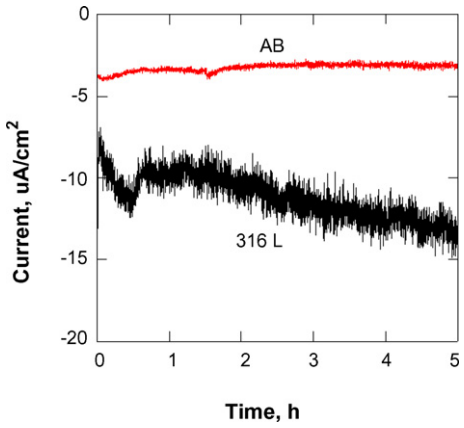

Fig. 17. Polarization current variation with time of 316L and AB alloy at a constant potential of −444 mV versus SCE in the acid solution bubbled with H_2 at 80 °C.

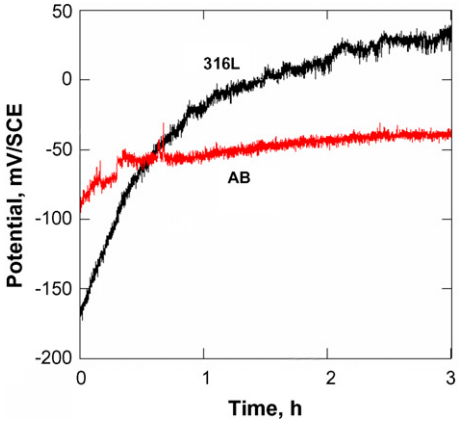

Fig. 18. Three hours potential decay of 316L and AB alloy after potentiostatic polarization at −444 mV versus SCE followed by 5 min potential decay in the acid solution bubbled with H_2 at 80 °C.

current was very high (25 μA cm^{-2}), quickly dropped to about 7.5 μA cm^{-2}, and later slowly increased to 14 μA cm^{-2}.

The potential decay was recorded immediately at the end of the potentiostatic polarization, as shown in Fig. 18. In the first 40 min, the E_{corr} of 316L was lower than that of AB which can be explained similarly as in the case of Fig. 10. After 40 min, the 316L corrosion potential became more positive than that of AB. The corrosion current of 316L was four times that of AB after 3 h of potential decay as shown in Table 5. This behavior corresponded to the oxidation of adsorbed hydrogen on the stainless steel surface. In summary, both materials were active during the cell shutdown period but no corrosion products were observed after 3 h of free corrosion following 5 h polarization.

Table 5
Corrosion potential and current, polarization resistance and corrosion rate after 5 h of potentiostatic polarization followed by 3 h potential decay in the acid solution bubbled with H_2 at 80 °C

Sample	E_{corr} (mV versus SCE)	i_{corr} (μA cm^{-2})	R_p (kΩ cm^2)	Rate$_{corr}$ (μm $year^{-1}$)
316L	34	0.087	249	1.01
AB	−40	0.021	1043	0.24

3.3.2.2. EIS results. Fig. 19 shows the Nyquist plots of the two materials polarized at −444 mV versus SCE obtained at the ends of 20 min (Fig. 19A) and 5.5 h (Fig. 19B) of polarization, respectively. It is seen from Fig. 19 that the semi-circle for AB is much bigger than that of 316L. Furthermore, the difference of the size of the two semi-circles corresponding to AB and 316L increases with polarization time. This means that AB always has a lower polarization current than 316L. As in the case of the DC polarization studies, higher polarization current on 316L indicated that the hydrogen ions were reduced (at the polarization potential) more easily in the case of 316L than AB, producing more adsorbed hydrogen on the electrode surface. Since the newly produced hydrogen atoms are very active and can reduce the passive layer, the higher polarization current means lower stability of the stainless steel than AB in these conditions.

However, in the acid solution bubbled with air under free corrosion conditions, the corrosion rate of 316L was lower than that of the AB. Under polarization conditions at 600 mV versus Ag/AgCl, the polarization current of AB was much higher than that of 316L; and after the polarization, the corrosion rates of AB were 12 and 255 times greater than those of 316L at 25 and 80 °C, respectively [21]. Thus, a double plate with stainless steel surface on one side for the simulated cathodic environment reaction (air) and AB alloy on the other side for the simulated anodic environment (hydrogen atmosphere) could give long and excellent performance as bipolar plate for PEMFC.

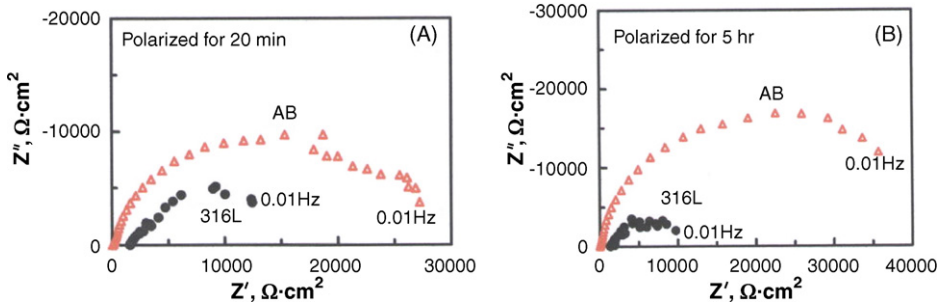

Fig. 19. Comparison of the Nyquist plots of 316L and AB alloy polarized at −444 mV versus SCE for 20 min (A) and 5.5 h (B), respectively, in the acid solution bubbled with H_2 at 80 °C.

4. Conclusions

From the results of this investigation, the following conclusion can be drawn:

- The 316L stainless steel in the acidic solution bubbled with H_2 at open circuit potential showed a more positive corrosion potential than the bulk amorphous $Zr_{75}Ti_{25}$ alloy. The corrosion rates of $Zr_{75}Ti_{25}$ alloy were 17% (for 20 h of immersion) and 43% (for 3 h of immersion) lower than those of 316L stainless steel at 25 and 80 °C, respectively.
- The 316L polarization current was higher than AB when the electrodes were polarized at −444 mV versus SCE (−400 mV versus Ag/AgCl). Longer experimental time is required to determine if the performance of the two alloys could change during extended service. Higher 316L polarization currents were mainly due to the rapid kinetics of the hydrogen ions reduction reaction and partially to the passive film reduction.
- The AB corrosion rate at free corrosion (3 h immersion) was lower than the 316L rate after potentiostatic polarization was stopped. Thus, AB performed better than 316L under conditions similar to cell shut down.
- The corrosion rates of both alloys in the acidic solution at 80 °C were much higher than those at 25 °C.
- The passive state of stainless steel could not be maintained in the presence of a reducing atmosphere (hydrogen) and the absence of an oxidant in the simulated anode environment. In air environment (oxygen) stainless steel showed better performance than the $Zr_{75}Ti_{25}$ bulk amorphous alloy.
- A double plate with stainless steel surface on one side for the simulated cathodic environment reaction (air) and alloy AB on the other side for the simulated anodic environment (hydrogen atmosphere) could give long and excellent performance as bipolar plate for PEMFC.

Acknowledgements

The authors are grateful of the support provided by GM for the realization of this work. The interest and help of Doctors Carl Fuerst and Paul Krajewski are also appreciated.

References

[1] R. Hornung, G. Kappelt, J. Power Sources 72 (1998) 20–21.
[2] R.C. Makkus, A.H.H. Janssen, F.A. Bruijn, R.K.A.M. Mallant, J. Power Sources 86 (2000) 274–282.
[3] D.P. Davis, P.L. Adcock, M. Turpin, S.J. Rowen, J. Power Sources 86 (2000) 237–242.
[4] J. Wind, R. Spah, W. Kaiser, G. Bohm, J. Power Sources 105 (2002) 256–260.
[5] H. Wang, M.A. Sweikart, J. Turner, J. Power Sources 115 (2003) 243–251.
[6] J. Sholta, B. Horland, J. Garche, in: O. Savadogo, P.R. Roberge (Eds.), New Materials for Fuel Cell and Modern Battery Systems II, Ecole Polytechnique de Montreal, Montreal, Canada, 1997, pp. 330–334.
[7] M.C. Li, C.L. Zeng, S.Z. Luo, J.N. Shen, H.C. Lin, C.N. Cao, Electrochim. Acta 48 (2003) 1735–1741.
[8] M.C. Li, S. Luo, C.L. Zeng, J.N. Shen, H.C. Lin, C.N. Cao, Corros. Sci. 46 (2004) 1369–1380.
[9] A.A. Hermas, K. Ogura, T. Adachi, Electrochim. Acta 40 (1995) 837–844.
[10] A.A. Hermas, M.S. Morad, K. Ogura, Corros. Sci. 41 (1999) 2251–2266.
[11] A.A. Hermas, K. Ogura, Electrochim. Acta 41 (1996) 1601–1609.
[12] H. Wang, J.A. Turned, J. Power Sources 128 (2004) 193–200.
[13] M.P. Brady, K. Weisbrod, I. Paulauskas, R.A. Buchanan, K.L. More, H. Wang, M. Wilson, F. Garzon, L.R. Walker, Scr. Mater. 50 (2004) 1017–1022.
[14] B.E. Conway, L. Bai, Int. J. Hydrogen Energy 11 (1986) 533–540.
[15] A. Iversen, Corros. Sci. 48 (2006) 1036–1058.
[16] K. Juttner, Electrochem. Acta 35 (1990) 1501–1508.
[17] B.E. Conway, L. Bai, Electrochem. Acta 31 (1986) 1013–1024.
[18] B.E. Conway, L. Bai, J. Electroanal. Chem. 198 (1986) 149–175.
[19] P. Gu, L. Bai, L. Gao, R. Brousseau, B.E. Conway, Electrochem. Acta 37 (1992) 2145–2154.
[20] L. Gao, Interface 2 (1993) 58–59.
[21] S. Jin, E. Ghali, A. Morales, General Motors, Laval University, Final Research Report, March 2005.